Progress on the realisation of high-resolution thin monolithic shells

M.M.Civitani[a,*], S.Basso[a], V.Cotroneo[a], M.Demmer[b], M.Ghigo[a], S.Incorvaia[c], L.Lessio[d], G.Pareschi[a], G.Parodi[e], E.M.A.Redaelli[a], S.Schuler[b], D.Spiga[a], G.Toso[c], and G.Vecchi[a]

[a]INAF-OABrera, Via E. Bianchi 46, 23807 Merate (LC), Italy
[b]LT Ultra-Precision Technology GmbH, Wiesenstr. 9,D-88634 Aftholderberg, Germany
[c]INAF-IASF, Via E. Bassini 15, 20133 Milano, Italy
[d]INAF-OAPd, Vicolo dell'Osservatorio 5, 35122, Padova (PD), Italy
[e]BCV Progetti, Via S. Orsola 1, 20123 Milano, Italy

ABSTRACT

An X-ray Observatory, with superb imaging capabilities and with large throughput, has been recognised as a strategic missions in the Astro2020 decadal survey. The traditional solution foreseen for the realisation of very large x-ray mirror modules (diameters above 1 m) is the partition of the optics in azimuthal and radial modules (like Silicon Pore Optics in Athena). Even if this approach solves the initial problem of the procurement and the handling of very large substrates, it moves the difficulties in the second phase, when thousands of segments have to be assembled without degrading their optical performances. On the contrary, a simpler large mirror module design could correspond to less than a few hundred thin monolithic shells. As an example, the complete opto-mechanical design, compliant with the Lynx mass budget and based on fused silica, foresees that the shell thickness ranges between 2 and 4 mm (for mirror shells between 0.4 and 3 m diameter). The conceptual design of such an mirror module could be refined for smaller scale mission, keeping both the advantage of the design simplicity and of the high-resolution capability, achievable through the direct polishing approach. A technology development roadmap for this approach is funded in Italy by ASI and led by INAF-OAB. In this paper, we present the advancements obtained in the development of the different phases of the process and in the realisation of two new single-reflection shells (SR shells), almost representative of the final optical configuration foreseen for the mirror assembly. The first shell will be used to prove the figuring process in a lab-mount, built upon elements of the previous supporting structure concept. The second shell will be hosted in an upgraded lab-mount structure, which guarantees better performances (frequencies, gravity and thermo-elastic response) and which is suitable to test the transfer of the shell to a spider-like configuration.

Keywords: Lynx, X-ray optics, fused silica, full shell, direct polishing, ion beam figuring

1. INTRODUCTION

High-angular resolution X-ray optics were established in the 1990's with the Chandra X-ray Observatory.[1] Its mirror module was based on four full-shell mirror pairs with an exquisite angular resolution < 0.5 arcsec HEW. The mirrors were 1.6 - 2.4 cm thick made of Zerodur. They were fabricated combining a very accurate metrology to standard grinding and polishing techniques. As a drawback, due to their mass, they provide a relatively modest effective area at 1 keV (0.11 m^2).

The Full Shell Optics technology pursued at INAF-OABrera is based on the same concept but, in this case, with the grinding, polishing, super-polishing of very thin monolithic mirror shells. An additional ion beam figuring final correction could further improve the shell optical quality.[2–4] Previous efforts on the direct fabrication of fused silica full shells started in 2010 by the Brera Astronomical Observatory.[5] In that case, primary and secondary surfaces were adjacent. The shells were characterised by a small length-to-diameter aspect ratio and by the polynomial Wolter-like profile adopted for WFXT. A prototypal shell was realised in 2012, providing around 17 arcsec HEW.[6] Starting from a raw ground fused silica shell produced by HERAEUS (Germany), a

Contact author: marta.civitani@inaf.it

Space Telescopes and Instrumentation 2022: Ultraviolet to Gamma Ray, edited by Jan-Willem A. den Herder, Shouleh Nikzad, Kazuhiro Nakazawa, Proc. of SPIE Vol. 12181, 1218112 · © 2022 SPIE · 0277-786X · doi: 10.1117/12.2628982

double-cone shell was fine ground in collaboration with LT-Ultra GmbH in Germany. A deterministic figuring process was then applied by means of IRP600 Zeeko machine based on bonnet polishing in order to impose the polynomial Wolter-like profile.[7] Then, the super polishing process was implemented using a dedicated pitch tool mounted on the IRP600 robotic arm.

The feasibility of such a process has been explored recently in relation to the Lynx mission[8] . In particular, to meet the effective area, the angular resolution and the grasp requirements, while remaining within system-level mass and geometry contingency reserves, the Lynx Mirror Assembly (LMA) design[9] required at least an order of magnitude thinner mirror substrates with respect to the Chandra's mirrors. The LMA opto-mechanic design is based on fused silica shells. This material has adequate mechanical and thermal properties: low density ($2.2g/cm^3$), low thermal expansion coefficient ($0.5 * 10^{-6}/K$) and a good modulus of elasticity ($70GPa$). In order to increase the effective area without exceeding the system level mass constraints, the shells are very thin compared to the diameter. Thicknesses range between 1.6 mm and 3.4 mm for shell diameters between 400 mm and 3000 mm. The realisation of these thin mirrors takes advantage of the intrinsic stiffness of the monolithic axial-symmetric shells and adopts an ad-hoc integration concept based on a Shell Supporting Structure (SSS) jig, used for the handling and to support the shell in all the manufacturing steps up to the integration into the Final Spoke Wheel (FSW). The primary and secondary optical surfaces are realised independently. Therefore, two separate conical blanks have to be procured, figured and coated. Next they are co-aligned during the integration into the FSW.

In this paper we describe the advancements on the two main goals of the current work-program: (1) test and optimisation of the figuring on single reflection shells, (2) test the transfer to a spoke-wheel-like structure.

2. RAW SHELLS

According to the opto-mechanical design deeply studied for full shell approach, the primary and secondary optical surfaces are realised independently. So, two separate conical blanks have to be procured for each of the double-reflection shells. Keeping the same shell thickness range, the shell length can be adapted to the requirements of the target mission. If a large Grasp is required, the lenght of the shell is necessarily short, but may be increased to improve the area/mass ratio if the desired optical performances are not extremes.

In the past, raw fused silica shells were purchased by OAB from Heraeus Quarzglass GmbH & Co KG. Starting from cylindrical tubes, a raw grinding process was applied in order to obtain shells in double conical configuration, with diameters in the 400 - 600 mm range, focal length of 5 m and total lengths of 200 - 270 mm. The typical profile errors after grinding were in the order of 50 microns peak-to-valley. Cylindrical blanks with diameters up to 900 mm and wall thicknesses between 0.5 - 13 mm could be purchased from this vendor. We are currently evaluating new supply chain for the grinding process making cylinders into cones, as this process is no more available at Hereaus. Other vendors may provide fused silica shells, including Corning Incorporated (USA). In this respect, the realisation of very large diameter shells (up to 3 m) is already in the capabilities of this company. For this scope, the conical shells are cut via water-jet from a chunk of fused silica and then ground. Due to the shell costs, the procurement of new blanks is still pending. It will be evaluated with respect to the funding time-line.

Figure 1a and Figure 1b show the optical design for the mirror shell under realisation. It is compatible with the available fused silica raw shells and takes into account the removal of around 100 micron from the surface to get the final optical surface, in a Wolter-Schwarchild design. The complete primary reflective surface is shown in red, while the secondary is in blue. The single reflection shell section is drawn in cyan. The length of the surface is 126.4 mm and radius range between 245.2 mm and 247.7 mm. The focal length of the designed surface (assuming double reflection) is 5000 mm. A gap of 140 mm is left in the intersection plane direction in view of integration into a SW. With these assumptions, the amount of material to be removed for getting to the theoretical shape is almost homogeneous. It ranges between 157 and 170 micron along the longitudinal axis and it gives enough margin for correcting out-of-roundness/integration errors.

In order to overcome the problem of expensive and fragile raw shell procurement, metal shell can be also used, at least in a first phase, in order to verify the set-up, test the integration procedures and validate the mechanical model. In Table 1 we report the properties of different materials which could be used. Taking into account the

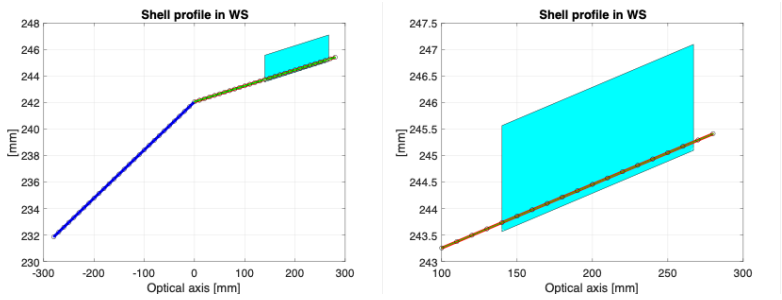

(a) (b)

Figure 1: (a) Primary and secondary Wolter-Schwarchild profiles, with the radial section of the shell FS-01. (b) Details of the theoretical design and the initial measured shell geometry.

Table 1: *Mechanical properties of the materials used in the analysis*

	Density $[g/cm^3]$	Young's modulus $[Gpa]$	Poisson Ratio	CTE $[m/(m*K)]$	Thermal Cond. $[W/(m*K)]$	Specific Heat $[J/(kg*K)]$
Fused silica	2.201	70	0.17	5.1∗10−7	1.38	772
Invar	8.05	148	0.3	1.3∗10−6	10.15	515
Al. 6082	2.7	70	0.3	24∗10−6	170	900

realisation costs, the most appealing material is aluminium. Moreover, due to the similarity of Young's modulus and of density, aluminium has almost the same mechanical behaviour of glass, except for CTE. Nevertheless, the large difference in CTE is mitigated by thermal conductivity. As explained before, these shells can be used in a very first phase for procedure validation. In particular, it will be very helpful to test the integration procedure of the shell into the SW using a low cost mock up instead of an expensive and brittle glass workpiece.

In order to have a representative mock up of the mirror shells, the plate turning technique has been explored.[10] Being a replica process, several mock up can be realised with the same mandrel without degradation. The maximum size of the realised shells depends on the dimensions of initial metallic plates. The shaping of parts up to 5 m diameters is already within the capabilities of some companies (e.g. Giotto Fratelli S.r.l, Italy). Figure 2a and Figure 2b show raw shells in fused silica and in aluminium, respectively.

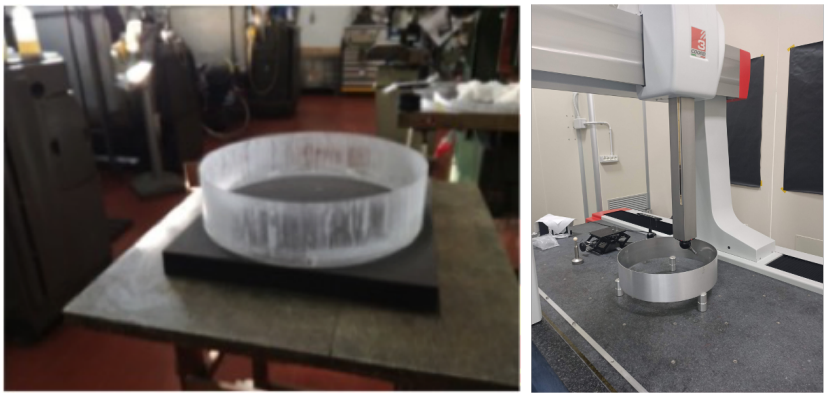

(a) (b)

Figure 2: (a) One of the three single reflection shells obtained by cutting the double reflection configuration shells. (b) An aluminium shell under measurement with coordinate measurement machine.

3. FIRST SINGLE REFLECTION SHELL FIGURING

The activities on the first Single Reflection shell SR_01 started in October 2021, when the shell was integrated into the temporary supporting system, hereafter S2. The shell is oriented with respect to the S2 support so that PhiMax is near the Invar spoke wheel and PhiMin in the external section. Details of the integration procedure are shown in . The S2 was placed on a rotary table and aligned with respect to the rotation centre. The astatic support was fixed directly to the Invar spider.[11] After the actuators calibration, the shell was positioned and centred with respect to the system. Given the density of the RTV566 and the reduced thickness required, it was not possible to flow the adhesive between the flexures and the glass without moving or deforming the shell. Therefore, the shell movements were limited by means of regulable screws in few points before starting the adhesive distribution. Thanks to the Ivar magnetic behaviour, it was possible to retract the flexures to distribute the adhesive directly on the flexure. Then, the final positioning of the flexures was reached by means of the regulable screws. This workaround solution will not be necessary with the new S3 system under realisation, with a great simplification of the bonding scheme, granting better thickness homogeneity and flexures positioning accuracy. Furthermore, an epoxy with a lower density is foreseen for the future shell. Figure shows the S2 with the shell on the astatic support and the measurements results in terms of Out Of Roundness (OOR) recorded on the shell central section before and after the bonding. The initial shape is almost preserved with the 'fixation'. The adhesive distribution changed slightly the shell shape so that the residual errors in terms of PtV is almost unvaried.

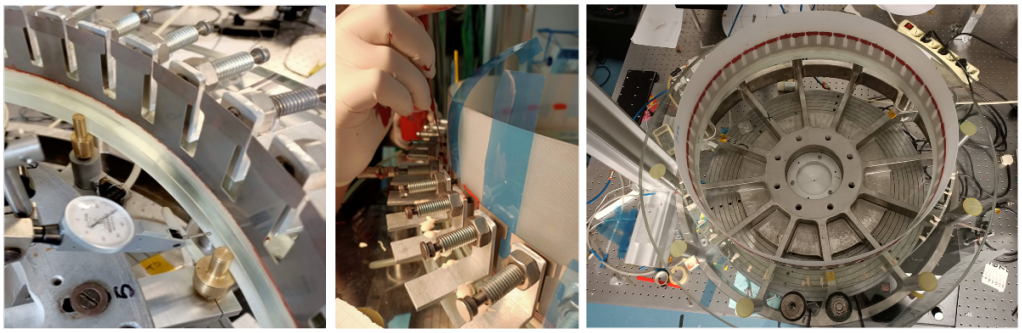

(a) (b) (c)

Figure 3: (a) Details of the Invar flexures system. (b) The distance between the flexures and the glass shell is controlled with plastic spacers. (c) The shell after the fixation to the S2.

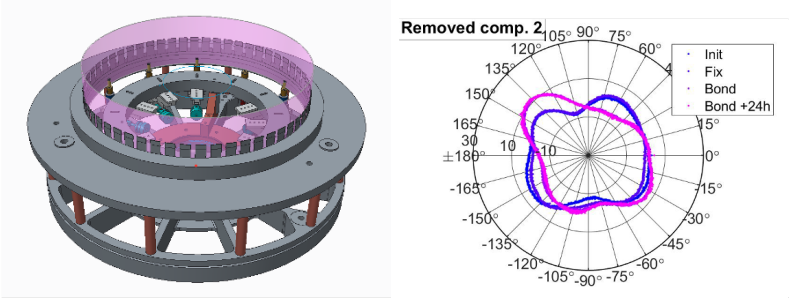

(a) (b)

Figure 4: (a) The shell integration scheme into the S2. (b) The OOR measured on the shell during the integration process: on the astatic support, once fixed to limit movements, after the bonding and during adhesive curing.

The figuring of the shell started according to the machine availability at the end of May 2022. An handling tool was prepared by INAF-OABrera: it was designed with a central tube to be connected to the S2 spider, in such a way to absorb possible deformations, leaving unvaried the shell support system and the shell. The shell in the S2 was cleaned, attached to the new handling system and then fixed to the lathe interface. Figure 5a shows two handling tool operations. On the left, we show the initial configuration, with shell optical axis in vertical

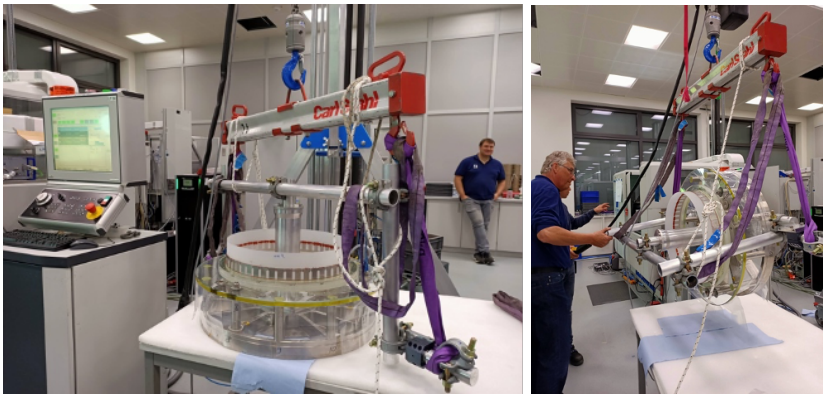

(a) (b)

Figure 5: The handling tool used to install the shell on the lathe. A central tube is connected to the spider and is used as connection to the system, so that no deformation is expected on the shell support system. a) Initial configuration, with shell optical axis in vertical direction. (b) Ready for the transfer, with the shell optical axis in horizontal direction.

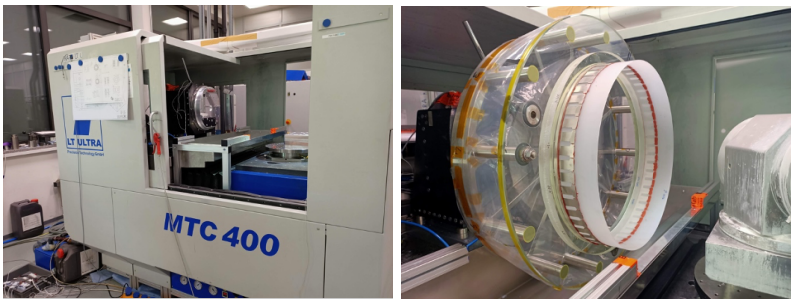

(a) (b)

Figure 6: (a) Diamond turning lathe installed at LT-Ultra. (b) The shell in the S2 installed on board of the lathe. Plastic covers limit the liquid dispersion.

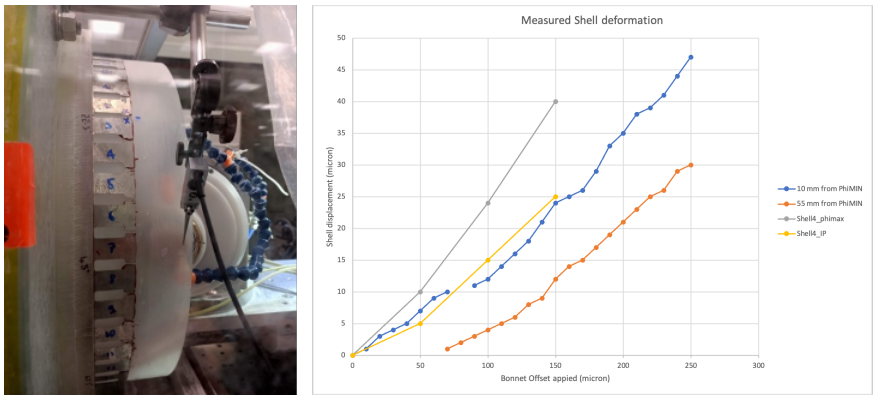

(a) (b)

Figure 7: (a) Shell deflection measurement set-up. (b) Measured deformation on the back surface of the shell under machining in two different accessible positions, near the edge and near the flexures. Data are compared with the ones acquired on previous shell#4.

direction. On the right, the shell is rotated and ready for the transfer, with the shell optical axis in horizontal direction.

Figure 6a shows the diamond turning machine used for the machining. A metallic box was designed and installed under the rotary table to collect the liquids and prevent machine damage. Even if its shape was studied to mitigate slurry sedimentation, we encountered some problems in controlling the slurry density during the

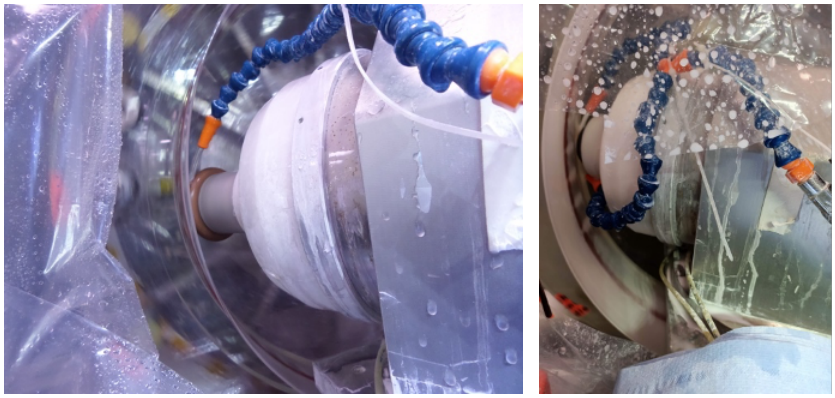

(a) (b)

Figure 8: (a) The grinding wheel operating on the shell during a grinding run on the lathe. (b) Details of the 'Bonnet' polishing phase operated on the lathe. Two nozzles distribute the slurry on the the surface and on the bonnet.

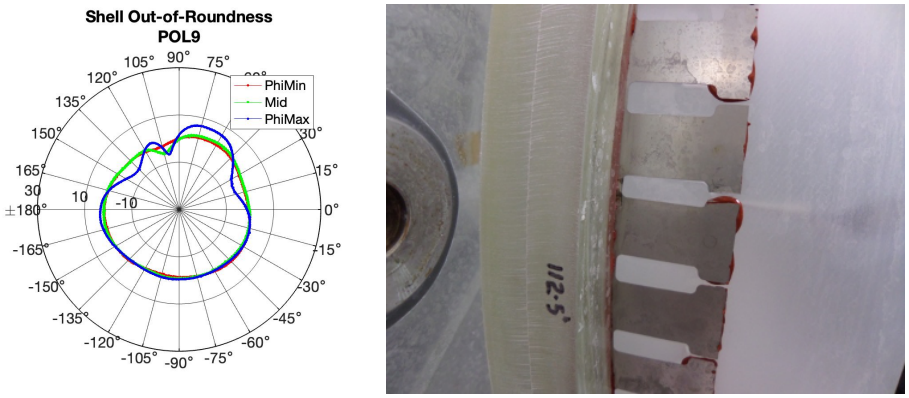

(a) (b)

Figure 9: (a) The final OOR acquired on the shell surface, measured top, middle and bottom of the shell. A defects is visible at the level of the central measurement and it increases its amplitude toward Phimax. (b) In correspondence of the measured shell distortion, the flexure strip is not properly overlapping, which could impact on the flexure mechanical behaviour.

process. Further optimisation is foreseen for the activities on future shell. The S2 was fixed initially by means of 4 screws and then after the removal of the central interface of the handling tool with the other 4 screws. Figure 6b reports the final configuration for the shell on the lathe machine. Plastic sheets were fixed to the S2 to limit the liquid spreading over during the operations.

As the shell is just 2 mm thick, we need to take into account its flexibility during the figuring operations. In order to effectively shape the surface, the different tools (grinding wheel, bonnet, pitch pad) need to operate on the surface with an offset with respect to the original position of the shell surface. Despite that larger offset may correspond to higher efficiency of the process, in particular during the polishing phase, larger deformations may be critical for the shell safety. We relied on FEA simulations to set the shell safety constraints. According to the model, the maximum deformation accettable by the shell should be < 50 microns. Figure 7a shows the set-up of measure the deflection. Data were acquired applying an offset with the Bonnet tool. Figure 7b reports the acquired values on FS_01 in the accessible positions (near Phimin and near the flexures), in blue and in orange respectively. The shell is stiffer near the flexures, so that higher deformation are near the edges. Data acquired for shell#4 are shown for comparison. In that case, larger deformations correspond to the same offset, limiting the process efficiency. This results is a combination of the shell reduced length and of the position of the flexure with respect to the shell length. Nevertheless, we can expect that given the reduced length, similar results will be achievable on the FS_02, even if the flexure position will be slightly different.

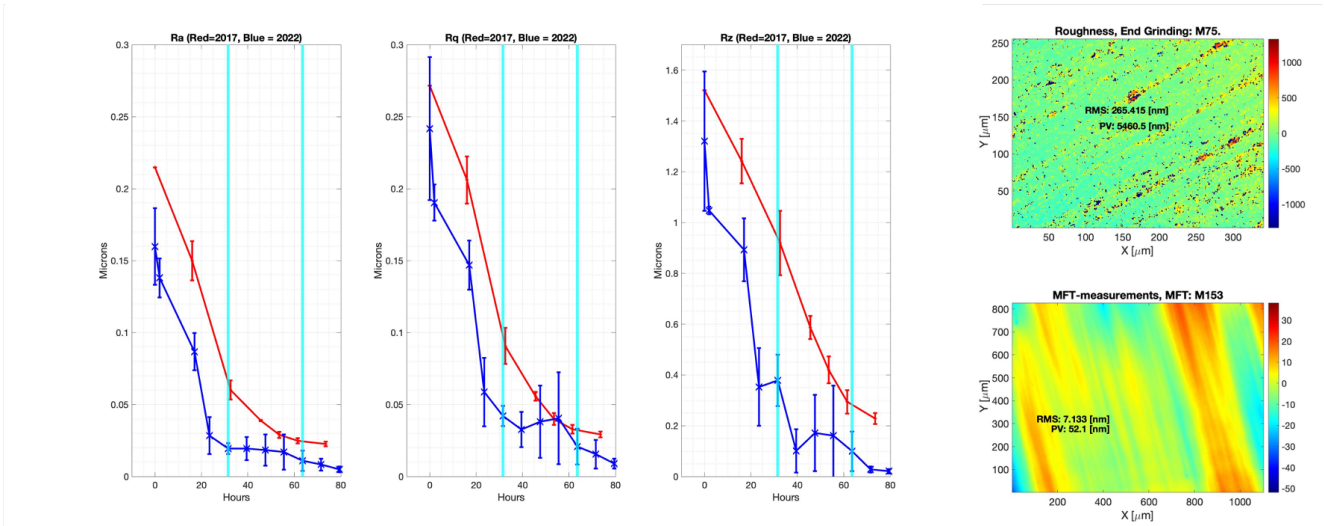

Figure 10: On the left, the micro-roughness evolution during the Bonnet polishing phase. Data acquired in 2017 on shell#4 are reported in red. Data relevant to the FS_01 are displayed in blue. Vertical lines in cyan indicate the changes in the process setting in the current figuring phase. Initially, the slurry density was kept around $1.006 g/cm^3$, the shell speed was 10 RPM and the offset 200 microns. Then we increased the density around $1.009 g/cm^3$ and the offset to 250 microns. In the last runs, we increased the shell speed to 15 RPM. On the right, two topography images of the shell surface, at the end of the grinding and at the end of the Bonnet polishing.

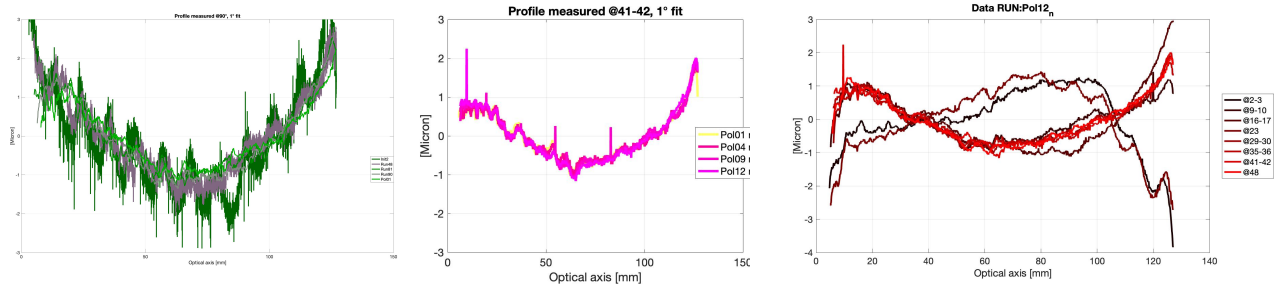

(a) (b) (c)

Figure 11: (a) The profiles acquired on a longitudinal section of the shell at different stages of the grinding phase (b) The longitudinal profiles acquired during Bonnet polishing phase. (c) The longitudinal profiles acquired in the different azimuthal directions at the end of the Bonnet polishing phase.

The grinding and the bonnet phases are shown in Figure 8a and 8b. The grinding phase was organised in 90 small runs, each of them lasting around 20 min. We operated with a single grinding wheel D20. Up to run 48, the shell and the grinding wheel were rotating in the same direction. This configuration improves the surface micro-roughness but slows down the process. Therefore, the standard opposite rotation direction was restored. The OOR correction was effective on a large part of the shell, but in a localised azimuthal area a deformation was not corrigible. Figure 9a shows the last OOR profiles acquired on the shell. The deformation starts in the central position near the flexure and increase in amplitude in Phimax direction. It appears with reduced amplitude in Phimin direction. In the same azimuthal position, in correspondence of the deformation, there is a join of the flexures strip which was not well realised, introducing some un-controlled effect on the shell shape, see Figure 9b. Given that it was not possible to improve the configuration, we stopped the grinding with a large azimuthal fraction of the shell within few microns. Masking the deformed part or measuring independently the different sections the shell will allow the cross-check with the metrological data, granting a correct interpretation of the shell surface optical quality.

The Sub Surface Damage removal was operated by means of a Bonnet tool R40 was mounted on the spindle. It rotates at 1000 rpm and CeO2 slurry distributed by means of two nozzles. The Bonnet polishing phase was

divided in 12 runs. Due to different procedural aspects under optimization, the initial runs were shorter. At regime, each of the run lasted 8 hours. In Figure 10 we show the micro-roughness evolution during the Bonnet polishing phases. The data acquired in 2017 on shell#4 are reported in red and were acquired with the Mahrr profiler. Due the low slurry density we could not improve the surface quality to the required level. The data relevant to the FS_01 are displayed in blue and were acquired with a replica approach and measured with New View. Vertical line in cyan indicates the changes in the process setting in the figuring relevant to the FS_01. Initially, the slurry density was kept around $1.006 g/cm^3$, the shell RPM was 10 and the offset 200 microns. Then we increased the density around $1.009 g/cm^3$ and the offset to 250 microns. In the last runs, we increased the shell RPM to 15. On the right, two images of the shell surfaces, at the end of the grinding (acquired with the NewView on a replica sample) and at the end of the Bonnet polishing (with Micro-Finish Topographer). It appears that higher slurry density and higher offset were effective in improving the surface in local areas, increasing the spread of the measurements. The last runs operated at higher shell rotational velocity were effective in homogenising the result on all the surface.

The longitudinal profiles acquired on the shell surface during different phases of the grinding are shown in Figure 11a. After the change in the relative rotation of the shell and of the grinding wheel at Run#48), the initial raw grinding pattern present on the shell started to be removed. The overall residual profile is a very low frequency error and was preserved apart in the area affected by the azimuthal deformation. Higher amount of material is removed in the PhiMin area, where the grinding runs start. Figure 11b shows the profiles evolution during the Bonnet polishing runs. The process appears very deterministic and the residual profiles remain unaffected by the process: the effects on the slurry density variation, which impact on the removal rate, are absorbed by the number of passages of the process. This feature opens the window to a possible profile correction by means of a 'moderation' of the transit velocity on the shell, slowing down when higher amount of material has to be removed. Given the local azimuthal deformation of the shell and the time spent in the process set-up, there was no more time to attempt the correction but it will be certainly explored with the future shell. The final status of the shell in terms of profile errors is shown in 11c in different azimuthal directions, which follow the flexure numeration. The residual profiles are quite similar in almost all the directions, except for the position where the azimuthal deformation affect completely the shell shape. The curvature of the shell is opposite in these areas and should not taken into account for a polishing/ion figuring future correction.

4. NEW LAB-MOUNT AND THE TRANSFER TO A SPIDER-LIKE STRUCTURE

A new support system, hereafter called S3, is under development. It will allow the figuring process of the second shell and its transfer to a spider-like structure. As for the S2, the S3 spoke wheel will interface with all the machines and devices to be used during manufacturing, metrology, testing, integration and x-ray calibration. In particular, it will be possible to separate the MS from the S3 just after the alignment and the connection to the final spoke wheel: the system is able to froze the initial low frequency errors on the shell so that their correction will remain effective after the transfer into the spider. The MS is fixed to the C-ring by a series of flexures, which provide low stiffness constraints in radial direction. On the contrary, the flexures provide stiff constraints in tangent and axial direction. The flexures can slide in radial direction on the C ring to adjust their distance from the MS. Once the correct distance is reached, the flexure sliders are fixed to the C-ring by screws and the adhesive can be injected in the gaps between flexures and MS. No additional forces can be applied to the flexures during this phase, since once removed they would give rise to spring back actions on the MS. During the bonding, the MS is supported on independent supports (the "astatic supports") at maximum diameter.[11] Once the adhesive between MS and flexures is cured, the astatic supports are removed, leaving the shell supported by the flexures in the S3. In this configuration the manufacturing operations can start.

FEM simulations were carried out to optimise the S3 performances, with respect to mechanical and thermal loads. The different configurations were judged against the frequencies, the MS distortions under gravity loads (1g axial or lateral) and the thermo-elastic distortions under assigned reference temperature distributions. The consequent impacts on optical degradation was evaluated by means of ray-tracing simulations. The final configuration foresees a spoke wheel with 12 spokes, which is connected to the C ring by 12 spacers, double T shaped, with flanges at both ends, to allows the bolted connections. The C ring accommodates 24 flexures to bond the MS (to be compared with 54 foreseen in the S2). Their radial position is adjustable in a range $\pm$ 3 mm. At the

upper end a thicker pad accommodates the interface for the adhesive spot (10 mm × 10 mm) used to connect the MS. The interface is conical shaped and the nominal adhesive thickness is equal to 300 μm. The spacer length is designed so that the shell bottom edge is 130 mm distant from the S3 and the MS top edge protrudes 30 mm from flexure end. The total mass of the assembly is 98.4 kg.

In general, once completed the figuring and the coating, the MS is ready to be aligned and connected to a Lab Spoke Wheel (LSW), a spider-like structure which mimics the final Fight Spoke Wheel (FSW). Then, the lab-mount structure is removed. We envisaged a dedicated equipment which was designed to guarantee alignment and bonding procedure of prototypal shell to the LSW. The new temporary supporting structure S3 has been designed to be compatible with this procedure. The LSW designed to support fused silica MS is made of INVAR and can be connected by three screws at its centre-hub to handling tools and testing fixtures. The MS is connected to each spoke by connectors, whose stiffness is customised on the basis of the LSW stiffness. The connectors are linked to the spokes by means of pins inserted and glued to tight tolerance holes. While the S3 allows small adjustment of the radial flexure position, so that it can accommodate MS having slightly different sizes, the FSW geometry needs to be customised on the basis of the actual MS size. Figure 12a shows the shell in the S3, while Figure 12b reports the shell in the S3 during the integration process. Figure 12c shows the final results. In the current design the total mass is approximately 42.5kg. As anticipated, for Aluminium alloy MS, the LSW and the connectors will be realised with the same material, avoiding CTE mismatch and reducing the cost. The resulting mass of the assembly composed by MS + LSW + connectors is much lower, approximately 15kg.

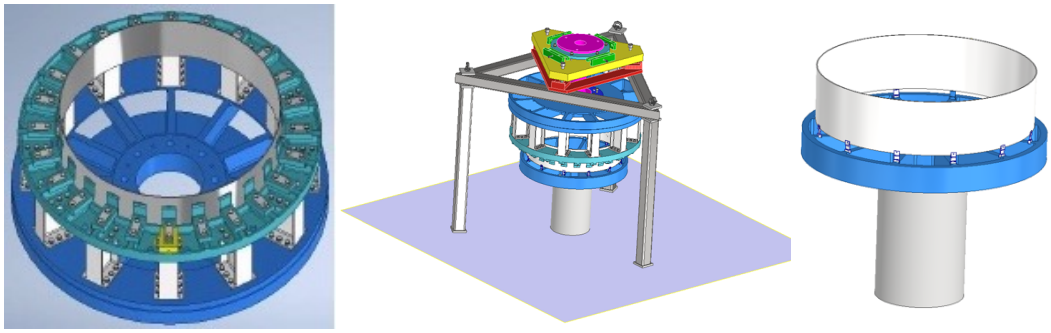

(a) (b) (c)

Figure 12: (a) Details of the Invar flexures system. (b) The distance between the flexures and the glass shell is controlled with plastic spacers. (c) The shell after the fixation to the S2.

FEA analysis, for both the nominal material selection (INVAR + SiO2 MS and full Aluminium case), were carried out to evaluate the behaviour of the system under gravity and thermoelastic loads. Fused silica + INVAR configuration shows better performances with respect to static thermal gradients effects, even if the highest contribution (in Aluminium case), due to axial gradient, can be corrected being associated to a change of focal length. Nevertheless, the 'full aluminium' performances are quite competitive, at least for a single MS, if the cost and the thermal conductibility are taken into account. In case residual elastic MS deformed shapes (cumulated during manufacturing/polishing and frozen by S3 flexures) existed, the MS would not be stress-free at the end of manufacturing. FEA simulations results suggest that the connection to the FSW is able to preserve such elastic deformed shapes with different efficiency. Two or three lobes deformed shapes in phase or out of phase are quite efficiently frozen, while higher azimuthal frequencies give rise to spring back gradually larger.

The adhesive is injected from the hole at the outer connector side. Since in the full telescope mirror assembly the inner volume is already filled by nested MS (integration will proceed from the innermost to the outermost MS), the inner MS surface is not easily accessible. For this reason, the connectors have a 'Bayonet' configuration. 'Bayonet' connectors (BC) are linked to the MS by adhesive just at the outer MS surface. In this way, we can assure a more reliable connection, avoiding the risk of incomplete adhesive filling at inner side.

To complete the preparation of the integration phase, a dedicated equipment has been designed to realise the transfer from the S3 to the FSW. The shell, integrated into the S3, is rotated 180° and fixed to the alignment tool

through the Invar spider. The displacement and the orientation of the shell are operated via the handling tool. All these equipments are under construction and should be ready before December 2022 to start the integration test activities.

5. CONCLUSIONS

The Full Shell Optics technology is based on direct polishing approach of thin monolithic fused silica shells. With an adequate selection of the thickness range, it is capable of combine effective area, angular resolution and grasp requirements while remaining within system-level mass and geometry contingency reserves. In this paper we have presented the on-going research activities. The figuring process of the single reflection shells, realised cutting the old double conical, is started and will be completed in few months. The grinding process and the bonnet polishing phases have been completed. We demonstrated the feasibility of the bonnet polishing on a modified diamond turning lathe. The remaining pitch polishing phase will be operated as soon as the machine will return available. The realisation of the new support system (S3), compatible with the single reflection configuration, is started and it will be assembled as soon as the procurement of all the parts will be completed. Then, the transfer from the temporary support to a spider-like structure will be tested. The promising results, provided by FEA simulations, will be cross-checked with prototypes figuring and integration in the next months.

ACKNOWLEDGMENTS

We thank the Italian Space Agency (ASI) for its support with a contract focused on glass shell development for X-ray optics (Accordo ASI INAF 2019-24-HH.0 - TAO-X: Tecnologie Avanzate per Ottiche in raggi X).

REFERENCES

[1] L.P.. Van Speybroeck, *et al.*, "Performance expectation versus reality," in *Proc. SPIE3113, 89-104*, **(1997)**.

[2] M.M. Civitani, *et al.*, "Lynx x-ray optics based on thin monolithic shells: design and development," *J. Astron. Telesc. Instrum. Syst* **5**(2), 021014 (2019).

[3] W. Liao, *et al.*, "Morphology evolution of fused silica surface during ion beam figuring of high-slope optical components," in *Applied Optics, Vol. 52, p. 3719-3725*, **(2013)**.

[4] M. Ghigo, *et al.*, "Development of a large ion beam figuring facility for correction of optics up to 1.7 m diameter," in *Proc. SPIE7426*, 742611 **(2009)**.

[5] L. Proserpio, *et al.*, "Design and development of thin quartz glass WFXT polynomial mirror shells by direct polishing," in *Proc. SPIE7732*, 77322OD **(2010)**.

[6] M.M. Civitani, *et al.*, "Thin glass shell oriented to wide field x-ray telescope," in *Proc. SPIE8443*, 84430Q **(2012)**.

[7] D.D. Walker, *et al.*, "Precessions process for efficient production of aspheric optics for large telescopes and their instrumentation," in *Proc. SPIE4451*, 267 **(2002)**.

[8] J.A.. Gaskin, *et al.*, "Lynx Mission concept status," in *Proc. SPIE10397, 103970S*, **(2017)**.

[9] M.M. Civitani, *et al.*, "Lynx optics based on full monolithic shells: design and development," in *Proc. SPIE1069911*, **(2018)**.

[10] M.M. Civitani, *et al.*, "A novel approach for fast and effective realisation of high-resolution x-ray optics in metal," in *Proc. SPIE11822, 1182227*, **(2021)**.

[11] M.M. Civitani, *et al.*, "Thin full shells oriented to the Lynx X-ray telescope: from design to breadboard realisation," in *Proc. SPIE111190T*, **(2019)**.